Towards CMOS-compatible nanophotonics: Ultra-compact modulators using alternative plasmonic materials

Viktoriia E. Babicheva,[1,2] Nathaniel Kinsey,[2] Gururaj V. Naik,[2] Marcello Ferrera,[2,3] Andrei V. Lavrinenko,[1] Vladimir M. Shalaev,[2,4] and Alexandra Boltasseva[1,2,*]

[1]*DTU Fotonik – Department of Photonics Engineering, Technical University of Denmark, Oersteds Plads 343, DK-2800 Kgs. Lyngby, Denmark*

[2]*School of Electrical & Computer Engineering and Birck Nanotechnology Center, Purdue University, 1205 West State Street, West Lafayette, Indiana 47907-2057 USA*

[3]*Also with the School of Engineering and Physical Sciences, Heriot-Watt University, David Brewster Building, Edinburgh, Scotland EH14 4AS, UK*

[4]*The Russian Quantum Center, Novaya Str., 100, BC "URAL", Skolkovo, Moscow Region, 143025, Russia*

[*]*aeb@purdue.edu*

Abstract: We propose several planar layouts of ultra-compact plasmonic modulators that utilize alternative plasmonic materials such as transparent conducting oxides and titanium nitride. The modulation is achieved by tuning the carrier concentration in a transparent conducting oxide layer into and out of the plasmon resonance with an applied electric field. The resonance significantly increases the absorption coefficient of the modulator, which enables larger modulation depth. We show that an extinction ratio of 46 dB/μm can be achieved, allowing for a 3-dB modulation depth in much less than one micron at the telecommunication wavelength. Our multilayer structures can be integrated with existing plasmonic and photonic waveguides as well as novel semiconductor-based hybrid photonic/electronic circuits.

OCIS codes: (250.5403) Plasmonics; (240.6680) Surface plasmons; (230.7370) Waveguides; (250.4110) Modulators; (250.7360) Waveguide modulators.

References and links

1. J. A. Dionne and H. A. Atwater, "Plasmonics: metal-worthy methods and materials in nanophotonics," MRS Bull. **37**(08), 717–724 (2012).
2. M. L. Brongersma and V. M. Shalaev, "Applied physics. the case for plasmonics," Science **328**(5977), 440–441 (2010).
3. V. J. Sorger, R. F. Oulton, R.-M. Ma, and X. Zhang, "Toward integrated plasmonic circuits," MRS Bull. **37**(08), 728–738 (2012).
4. M. L. Brongersma and P. G. Kik, *Surface Plasmon Nanophotonics* (Springer, 2007).
5. S. I. Bozhevolnyi, *Plasmonic Nanoguides and Circuits* (Pan Stanford Publishing, 2009).
6. P. Berini, "Long-range surface plasmon polaritons," Adv. Opt. Photon. **1**(3), 484–588 (2009).
7. A. Boltasseva, T. Nikolajsen, K. Leosson, K. Kjaer, M. S. Larsen, and S. I. Bozhevolnyi, "Integrated optical components utilizing long-range surface plasmon polaritons," J. Lightwave Technol. **23**(1), 413–422 (2005).
8. R. Charbonneau, N. Lahoud, G. Mattiussi, and P. Berini, "Demonstration of integrated optics elements based on long-ranging surface plasmon polaritons," Opt. Express **13**(3), 977–984 (2005).
9. R. Charbonneau, C. Scales, I. Breukelaar, S. Fafard, N. Lahoud, G. Mattiussi, and P. Berini, "Passive integrated optics elements based on long-range surface plasmon polaritons," J. Lightwave Technol. **24**(1), 477–494 (2006).
10. V. J. Sorger, Z. Ye, R. F. Oulton, Y. Wang, G. Bartal, X. Yin, and X. Zhang, "Experimental demonstration of low-loss optical waveguiding at deep sub-wavelength scales," Nat. Commun. **2**, 331 (2011).
11. V. S. Volkov, Z. Han, M. G. Nielsen, K. Leosson, H. Keshmiri, J. Gosciniak, O. Albrektsen, and S. I. Bozhevolnyi, "Long-range dielectric-loaded surface plasmon polariton waveguides operating at telecommunication wavelengths," Opt. Lett. **36**(21), 4278–4280 (2011).
12. T. Nikolajsen, K. Leosson, and S. I. Bozhevolnyi, "Surface plasmon polariton based modulators and switches operating at telecom wavelengths," Appl. Phys. Lett. **85**(24), 5833–5835 (2004).

#194460 - $15.00 USD Received 26 Jul 2013; revised 17 Oct 2013; accepted 18 Oct 2013; published 4 Nov 2013

13. T. Nikolajsen, K. Leosson, and S. I. Bozhevolnyi, "In-line extinction modulator based on long-range surface plasmon polaritons," Opt. Commun. **244**(1-6), 455–459 (2005).
14. J. A. Dionne, K. Diest, L. A. Sweatlock, and H. A. Atwater, "PlasMOStor: a metal-oxide-Si field effect plasmonic modulator," Nano Lett. **9**(2), 897–902 (2009).
15. W. Cai, J. S. White, and M. L. Brongersma, "Compact, high-speed and power-efficient electrooptic plasmonic modulators," Nano Lett. **9**(12), 4403–4411 (2009).
16. K. F. MacDonald and N. I. Zheludev, "Active plasmonics: current status," Laser Photon. Rev. **4**(4), 562–567 (2010).
17. A. Melikyan, N. Lindenmann, S. Walheim, P. M. Leufke, S. Ulrich, J. Ye, P. Vincze, H. Hahn, T. Schimmel, C. Koos, W. Freude, and J. Leuthold, "Surface plasmon polariton absorption modulator," Opt. Express **19**(9), 8855–8869 (2011).
18. A. V. Krasavin and A. V. Zayats, "Photonic signal processing on electronic scales: electro-optical field-effect nanoplasmonic modulator," Phys. Rev. Lett. **109**(5), 053901 (2012).
19. V. J. Sorger, N. D. Lanzillotti-Kimura, R.-M. Ma, and X. Zhang, "Ultra-compact silicon nanophotonic modulator with broadband response," Nanophotonics **1**(1), 1–6 (2012).
20. C. Huang, R. J. Lamond, S. K. Pickus, Z. R. Li, and V. J. Sorger, "A sub-λ-size modulator beyond the efficiency-loss limit," IEEE Photon. J. **5**(4), 2202411 (2013).
21. V. E. Babicheva, I. V. Kulkova, R. Malureanu, K. Yvind, and A. V. Lavrinenko, "Plasmonic modulator based on gain-assisted metal–semiconductor–metal waveguide," Photon. Nanostructures **10**(4), 389–399 (2012).
22. A. Melikyan, L. Alloatti, A. Muslija, D. Hillerkuss, P. Schindler, J. Li, R. Palmer, D. Korn, S. Muehlbrandt, D. Van Thourhout, B. Chen, R. Dinu, M. Sommer, C. Koos, M. Kohl, W. Freude, and J. Leuthold, "Surface plasmon polariton high-speed modulator," CLEO: 2013, OSA Technical Digest, paper CTh5D.2 (2013).
23. R. Thomas, Z. Ikonic, and R. W. Kelsall, "Electro-optic metal–insulator–semiconductor–insulator–metal Mach-Zehnder plasmonic modulator," Photon. Nanostructures **10**(1), 183–189 (2012).
24. A. Boltasseva and H. A. Atwater, "Low-loss plasmonic metamaterials," Science **331**(6015), 290–291 (2011).
25. P. R. West, S. Ishii, G. V. Naik, N. K. Emani, V. M. Shalaev, and A. Boltasseva, "Searching for better plasmonic materials," Laser Photon. Rev. **4**(6), 795–808 (2010).
26. C. Rhodes, S. Franzen, J.-P. Maria, M. Losego, D. N. Leonard, B. Laughlin, G. Duscher, and S. Weibel, "Surface plasmon resonance in conducting metal oxides," J. Appl. Phys. **100**(5), 054905 (2006).
27. G. V. Naik, and A. Boltasseva, "Semiconductors for plasmonics and metamaterials," Phys. Status Solidi RRL **4**(10), 295–297 (2010).
28. G. V. Naik and A. Boltasseva, "A comparative study of semiconductor-based plasmonic metamaterials," Metamaterials (Amst.) **5**(1), 1–7 (2011).
29. G. Naik, J. Kim, and A. Boltasseva, "Oxides and nitrides as alternative plasmonic materials in the optical range," Opt. Mater. Express **4**(6), 1090–1099 (2011).
30. G. Naik, J. L. Schroeder, X. Ni, A. V. Kildishev, T. D. Sands, and A. Boltasseva, "Titanium nitride as a plasmonic material for visible and near-infrared wavelengths," Opt. Mater. Express **2**(4), 478–489 (2012).
31. G. V. Naik, J. Liu, A. V. Kildishev, V. M. Shalaev, and A. Boltasseva, "Demonstration of Al:ZnO as a plasmonic component for near-infrared metamaterials," Proc. Natl. Acad. Sci. U.S.A. **109**(23), 8834–8838 (2012).
32. J. B. Khurgin and A. Boltasseva, "Reflecting upon the losses in plasmonics and metamaterials," MRS Bull. **37**(08), 768–779 (2012).
33. G. V. Naik, V. M. Shalaev, and A. Boltasseva, "Alternative plasmonic materials: beyond gold and silver," Adv. Mater. **25**(24), 3264–3294 (2013).
34. J. Narayan, P. Tiwari, X. Chen, J. Singh, R. Chowdhury, and T. Zheleva, "Epitaxial growth of TiN films on (100) silicon substrates by laser physical vapor deposition," Appl. Phys. Lett. **61**(11), 1290–1292 (1992).
35. E. Feigenbaum, K. Diest, and H. A. Atwater, "Unity-order index change in transparent conducting oxides at visible frequencies," Nano Lett. **10**(6), 2111–2116 (2010).
36. Z. Lu, W. Zhao, and K. Shi, "Ultracompact electroabsorption modulators based on tunable epsilon-near-zero-slot waveguides," IEEE Photon. J. **4**(3), 735–740 (2012).
37. V. Babicheva and A. Lavrinenko, "Plasmonic modulator optimized by patterning of active layer and tuning permittivity," Opt. Commun. **285**(24), 5500–5507 (2012).
38. A. Kerber and E. A. Cartier, "Reliability challenges for CMOS technology qualifications with Hafnium Oxide/Titanium Nitride gate stacks," IEEE Trans. Device Mater. Reliab. **9**(2), 147–162 (2009).
39. R. Chau, M. Doczy, B. Doyle, and J. Kavalieros, "Metal-gate electrode for CMOS transistor applications," US Patent 6 696 345, Feb. 24 (2004).
40. J. K. Brask, T. E. Glassman, M. L. Doczy, and M. V. Metz, "Method for making a semiconductor device having a high-k gate dielectric," US Patent 6 716 707, Sept. 30 (2004).
41. A. Emboras, R. M. Briggs, A. Najar, S. Nambiar, C. Delacour, P. Grosse, E. Augendre, J. M. Fedeli, B. de Salvo, H. A. Atwater, and R. Espiau de Lamaestre, "Efficient coupler between silicon photonic and metal-insulator-silicon-metal plasmonic waveguides," Appl. Phys. Lett. **101**(25), 251117 (2012).
42. B. Little, "A VLSI photonics platform," in *Optical Fiber Communication Conference*, (Optical Society of America, 2003), paper ThD1.

#194460 - $15.00 USD Received 26 Jul 2013; revised 17 Oct 2013; accepted 18 Oct 2013; published 4 Nov 2013

43. M. Ferrera, L. Razzari, D. Duchesne, R. Morandotti, Z. Yang, M. Liscidini, J. E. Sipe, S. Chu, B. E. Little, and D. J. Moss, "Low-power continuous-wave nonlinear optics in doped silica glass integrated waveguide structures," Nat. Photonics **2**(12), 737–740 (2008).
44. M.-S. Kwon, J.-S. Shin, S.-Y. Shin, and W.-G. Lee, "Characterizations of realized metal-insulator-silicon-insulator-metal waveguides and nanochannel fabrication via insulator removal," Opt. Express **20**(20), 21875–21887 (2012).
45. C. Delacour, S. Blaize, P. Grosse, J. M. Fedeli, A. Bruyant, R. Salas-Montiel, G. Lerondel, and A. Chelnokov, "Efficient directional coupling between silicon and copper plasmonic nanoslot waveguides: toward metal-oxide-silicon nanophotonics," Nano Lett. **10**(8), 2922–2926 (2010).
46. A. Emboras, A. Najar, S. Nambiar, P. Grosse, E. Augendre, C. Leroux, B. de Salvo, and R. E. de Lamaestre, "MNOS stack for reliable, low optical loss, Cu based CMOS plasmonic devices," Opt. Express **20**(13), 13612–13621 (2012).
47. S. Zhu, G. Q. Lo, and D. L. Kwong, "Electro-absorption modulation in horizontal metal-insulator-silicon-insulator-metal nanoplasmonic slot waveguides," Appl. Phys. Lett. **99**(15), 151114 (2011).
48. S. Zhu, G. Q. Lo, and D. L. Kwong, "Components for silicon plasmonic nanocircuits on horizontal Cu-SiO2-Si-SiO2-Cu nanoplasmonic waveguides," Opt. Express **20**, 1896–1898 (2012).
49. R. Geffken and S. Luce, "Method of forming a self-aligned copper diffusion barrier in vias," US Patent 5 985 762, Nov. 16 (1999).
50. K. Noguchi, O. Mitomi, and H. Miyazawa, "Millimeter-wave Ti:LiNbO3 optical modulators," J. Lightwave Technol. **16**(4), 615–619 (1998).
51. T. Fujiwara, A. Watanabe, and H. Mori, "Measurement of uniformity of driving voltage in Ti:LiNbO3 waveguides using Mach-Zehnder interferometers," IEEE Photon. Technol. Lett. **2**(4), 260–261 (1990).
52. J. Kim, G. Naik, N. Emani, U. Guler, and A. Boltasseva, "Plasmonic resonances in nanostructured transparent conducting oxide films," IEEE J. Sel. Top. Quantum Electron. **19**, 4601907 (2012).
53. M. Bass, C. DeCusatis, G. Li, V. N. Mahajan, and E. V. Stryland, *Handbook of Optics, Volume II: Design, Fabrication and Testing, Sources and Detectors, Radiometry and Photometry* (McGraw Hill, 1994).
54. Sopra data sheet, *http://www.sspectra.com/sopra.html*.
55. D. C. Look, T. C. Droubay, and S. A. Chambers, "Stable highly conductive ZnO via reduction of Zn vacancies," Appl. Phys. Lett. **101**(10), 102101 (2012).
56. M. A. Noginov, L. Gu, J. Livenere, G. Zhu, A. K. Pradhan, R. Mundle, M. Bahoura, Y. A. Barnakov, and V. A. Podolskiy, "Transparent conductive oxides: plasmonic materials for telecom wavelengths," Appl. Phys. Lett. **99**(2), 021101 (2011).
57. H. Kim, M. Osofsky, S. M. Prokes, O. J. Glembocki, and A. Piqué, "Optimization of Al-doped ZnO films for low loss plasmonic materials at telecommunication wavelengths," Appl. Phys. Lett. **102**(17), 171103 (2013).
58. B. Lamprecht, J. R. Krenn, G. Schider, H. Ditlbacher, M. Salerno, N. Felidj, A. Leitner, F. R. Aussenegg, and J. C. Weeber, "Surface plasmon propagation in microscale metal stripes," Appl. Phys. Lett. **79**(1), 51–53 (2001).
59. S. Kang and Y. Leblebici, *CMOS Digital Integrated Circuits Analysis & Designs* (McGraw Hill, 2003).

1. Introduction

Plasmonics enables the merging of two major technologies: nanometer-scale electronics and ultra-fast photonics [1]. Metal-dielectric interfaces can support the waves known as surface plasmon polaritons (SPPs) that are tightly coupled to the interface which allow for the manipulation of light at the nanoscale, overcoming the diffraction limit. Plasmonic technologies can lead to a new generation of fast, on-chip, nanoscale devices with unique capabilities [2, 3]. To provide basic nanophotonic circuit functionalities, elementary plasmonic devices such as waveguides, modulators, sources, amplifiers, and photodetectors are required. Various designs of plasmonic waveguides have been proposed to achieve the highest mode localization and the lowest propagation losses [3]. In addition to waveguides, modulators are the most fundamental component for digital signal encoding and are paramount to the development of nanophotonic circuits. In this regard, opto-electronic modulators can be designed to achieve operational speeds on the order of a few 10's of GHz. Many plasmonic waveguide and modulator structures have been proposed and experimentally verified, but most of these structures use metals such as gold or silver, which are not CMOS-compatible, limiting their applicability in realistic consumer devices [4–23].

Similar to the advances in silicon technologies that led to the information revolution worldwide, the development of new CMOS-compatible plasmonic materials with adjustable/tunable optical properties could revolutionize the field of hybrid photonic/electronic devices. Pioneering works in the search for new plasmonic materials [24, 25] have suggested new intermediate carrier density materials such as transition metal nitrides

#194460 - $15.00 USD Received 26 Jul 2013; revised 17 Oct 2013; accepted 18 Oct 2013; published 4 Nov 2013

and transparent conducting oxides (TCOs) as promising building blocks with low loss, and extraordinary tuning and modulation capabilities [26–33]. Among these materials, titanium nitride (TiN) is one of the best candidates for plasmonics applications due to its many intrinsic advantages [29, 30]. TiN is thermally stable (melting point above of 2900°C), bio-compatible, mechanically hard (one of the hardest ceramics), can be grown epitaxially on many substrates including [100]-silicon and [0001]-sapphire, and chemically stable; in particular, it does not oxidize like silver or copper [30, 34]. It was also shown that TiN provides higher plasmonic mode confinement in comparison to gold [28]. A final benefit of transition metal nitrides is that they are nonstoichiometric materials. Hence their optical properties depend greatly on the preparation conditions and can be optimized based on the desired application and performance. These unique properties make TiN a very promising material for telecommunication-range plasmonic waveguides.

TCOs can provide extraordinary tuning and modulation of their complex refractive indices by changing the carrier concentration with the application of an electric field [17–20, 35–37]. The resulting electric field causes a charge accumulation, or depletion, in the TCO layer (depending on the direction of electric field) which in turn changes the plasma frequency of the TCO, and consequently, its permittivity. In particular, an increase of approximately one order of magnitude can be achieved in a 5 nm thick accumulation layer for a metal-insulator-metal (MIM) structure using indium-tin-oxide (ITO) [35]. A similar decrease in the carrier concentration within a 10-nm thick film for metal-oxide-semiconductor (MOS) stack was demonstrated for an ITO film [19, 20]. The modulating speed is only RC limited and is expected to exceed 10's of GHz. TCO based modulators have been shown to achieve extinction ratios on the order of 18 dB/μm [36]. In addition, TCO permittivity tuning can provide further improvements and increase of propagation length [37]. A small absolute value of TCO permittivity can be utilized to achieve plasmonic resonances and consequently high extinction ratio [17, 36]. Thus, TCOs are promising candidates for adding electro-optical capabilities to plasmonic devices.

In this paper, we focus on developing active plasmonic devices using alternative plasmonic materials which are CMOS-compatible (Section 2). We suggest a variety of plasmonic modulator structures using transparent conducting oxides, which may serve as both the plasmonic material and as a dynamic element in Section 3. Next, a definition of the parameters used in the simulations is discussed in Section 4. Following, we define our figure of merit (FoM) and discuss results for the absorption coefficient and mode size as functions of the carrier concentration in the TCO layer in Section 5. The performance analysis of the modulators and previous works are shown in Section 6. Finally, we investigate the integration of the best performing modulator with plasmonic waveguides, and analyze its performance in terms of coupling losses and integration possibilities in Section 7.

2. Towards fully CMOS-compatible plasmonics

For a device to be fully CMOS-compatible, both the material and the processing technique used to synthesize this material should be compatible with the standards in CMOS production lines. Currently, TiN is routinely used in CMOS processing, but the optical properties of this material are quite poor [38–41]. This is because the primary consideration has been the electrical properties of the material, not the optical properties. In this study, we use experimentally obtained optical properties of TiN films which have been optimized for plasmonic applications [30]. These films were deposited using a high temperature (800 °C) reactive DC magnetron sputtering technique. This high temperature sputtering process is not utilized in the current semiconductor manufacturing processes for TiN deposition. Thus, we claim devices based on CMOS-compatible materials, but acknowledge that the entire process is not currently CMOS-compatible. However, it has been shown that plasmonic TiN can also be grown at lower temperatures [30, 33]. Thus, through an optimization process of the low temperature TiN (less than 400°) currently available in the CMOS industry, TiN which

#194460 - $15.00 USD Received 26 Jul 2013; revised 17 Oct 2013; accepted 18 Oct 2013; published 4 Nov 2013

possesses the required optical properties can be made available in future CMOS production lines. This is in stark contrast to the noble metals which are not allowed in the CMOS process. A similar situation was encountered for low-loss doped silica glass which is normally obtained through high-temperature annealing. Nevertheless, in 2003 a new material platform, namely Hydex®, was synthesized to bring this glass into full CMOS-compatibility where it was subsequently used for integrated nonlinear optics experiments [42, 43].

Copper has also been investigated as a potential CMOS-compatible plasmonic material [41, 44–48]. However, the use of copper first requires a TiN buffer layer to prevent its diffusion into silicon [49]. Thus, if the low-temperature TiN is optimized with competitive optical properties, the second deposition of copper is not necessary. TiN, in its own right, also has many advantages (as was previous discussed) over copper such as chemical and mechanical stability, high temperature stability and bio-compatibility, which are useful for many applications beyond only CMOS chips.

The TCOs discussed in this paper, Tin-doped Indium Oxide (ITO), Gallium-doped Zinc Oxide (GZO), Aluminum-doped Zinc-Oxide (AZO) and others, may be deposited at relatively low temperatures (less than 300°C), which makes it possible to integrate them as a final stage in the standard silicon process [31]. Due to their low temperature deposition they will not impact the CMOS produced structures below. Similar nondestructive methods of integration with CMOS circuitry have been utilized to include lithium niobate crystals and electro-optic polymers on CMOS produced photonic chips [50, 51]. Such methods also consider these techniques to be CMOS-compatible.

3. Multilayer structures

We consider the use of the above mentioned CMOS-compatible materials in several modulator configurations. Stripe waveguides have low propagation loss and are relatively simple to fabricate using the planar process [6, 7]. Therefore, we propose several modulator geometries which are based on stripe waveguides. This also allows for the modulator to be easily integrated with long-range SPP (LR-SPP) stripe waveguides [6] to decrease both propagation and coupling losses, leading to a fully plasmonic integrated modulator design. A schematic showing the basic outline of the modulator integration with LR-SPP stripe waveguides is shown in Fig. 1.

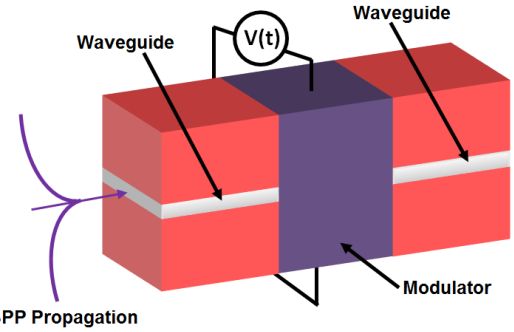

Fig. 1. General scheme of a compact modulator integrated with low-loss plasmonic waveguides. In this geometry, a stripe waveguide (grey) is used to bring a long ranging SPP mode to and from the modulator structure where an applied voltage modulates the SPP wave.

Within the modulator structure, three options are possible for the guiding layer. First, since TCOs possess plasmonic properties in the near-infrared range [25,33], a thin layer of TCO can be used to simultaneously support SPP propagation and control the attenuation of the signal. TCOs such as ITO, GZO and AZO have very similar optical properties and allow for efficient control of the carrier concentration. We select GZO for all structures as it possesses the highest plasma frequency [52]. Secondly, a thick layer of TiN can be used to

#194460 - $15.00 USD Received 26 Jul 2013; revised 17 Oct 2013; accepted 18 Oct 2013; published 4 Nov 2013

support a single interface SPP inside the waveguide while an upper TCO layer is used to control the attenuation. Lastly, a thin TiN layer, identical to the input/output waveguide, can be used to support the SPP inside the modulator, while an additional upper TCO layer is used to control the attenuation. The final two approaches simplify the fabrication of the structure while providing tighter modal confinement and a second electrode. However, it is not readily clear which solution will provide the best FoM. In the paper several structures which utilize these configurations will be investigated.

To further reduce the mode size of the three alternatives and increase the modulating capability, we consider including high-index claddings. However, due to the increased propagation losses in the modulator it is unclear whether structures with a high-index cladding will outperform the low-index equivalents. For this reason, we consider two sub-groups of devices: one with low-index claddings Figs. 2(a)-2(c), and another with high-index claddings Figs. 2(d)-2(f). In all structures, thin plasma-enhanced chemical vapor deposition (PE-CVD) nonstoichiometric silicon nitride (SiN) or thin low-pressure chemical vapor deposition (LP-CVD) Si_3N_4 layers, are used for electrical isolation between the contacts to allow for modulation.

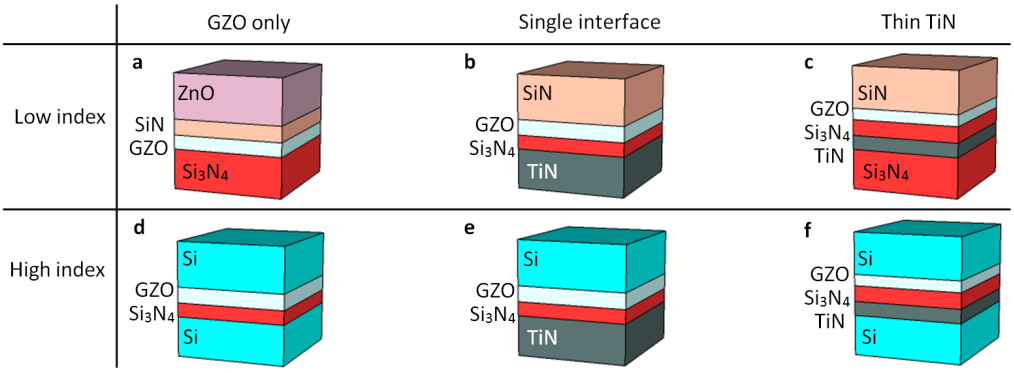

Fig. 2. Illustration of the low-index (a, b, c) and high-index (d, e, f) multilayer modulator designs considered in this work. They are vertically divided by their configuration. The first column, GZO only structures (a) and (d), uses the GZO as both the plasmonic layer and the dynamic layer. The second column, single interface structures (b) and (e), introduces a thick TiN layer, which supports single interface SPPs and use the GZO layer to perform modulation. Finally, the third column of thin TiN structures (c) and (f), uses a thin stripe of TiN to support the long ranging SPP mode and the GZO layer to modulate the signal.

4. Defining performance metrics

With these considerations, six basic geometries were chosen as templates for modulator designs, operating at the telecom wavelength of $\lambda = 1.55$ μm. We consider zinc oxide (ZnO), LP-CVD Si_3N_4 and PE-CVD silicon nitride (denoted in by SiN), as low-index materials. The refractive indices used in the calculations are the following: $n_{ZnO} = 1.93$ [53], $n_{SiN} = 1.76$ and $n_{Si3N4} = 1.97$ (value retrieved from in loco ellipsometry measurements of PE-CVD and LP-CVD films, respectively) at $\lambda = 1.55$ μm. It should be mentioned that LP-CVD Si_3N_4 requires high temperature deposition which may degrade the properties of TCO layer. Hence, only PE-CVD SiN can be deposited after the TCO layer. We consider silicon as a high-index cladding $n_{Si} = 3.48$ at $\lambda = 1.55$ μm for both crystalline and amorphous [54]. In all cases we neglect optical losses in the silicon as they are much lower than losses associated with plasmonic structures.

The dispersion equation was solved for the multilayer structures with varying carrier concentrations in the TCO. The permittivity of the GZO layer was taken from experimentally grown films [52] and a carrier concentration in the GZO was determined using a Drude-Lorentz model fitting: $N_0 = 9.426 \times 10^{20}$ cm^{-3}. For this work we consider a range of carrier

#194460 - $15.00 USD Received 26 Jul 2013; revised 17 Oct 2013; accepted 18 Oct 2013; published 4 Nov 2013

concentrations between $N = 0.5N_0 \ldots 2N_0$. The upper limit of $2N_0$ (1.88×10^{21} cm^{-3}) is shown to be achievable by the recently reported film which obtained a carrier concentration of 1.46×10^{21} cm^{-3} for GZO [55]. In addition, numerous studies have focused on increasing the carrier concentration of TCO films which is further proof that the parameters used in our analysis are realistic [33, 52, 55–57]. The calculated permittivity of GZO for these carrier concentrations is shown in Fig. 3(a).

The permittivity of TiN is taken as experimentally measured $\varepsilon_{TiN} = -83.3 + 21.3i$ at $\lambda = 1.55$ μm, Fig. 3(b). The TiN film was deposited at 800°C and the optical properties of the 20 nm thick film was measured using spectroscopic ellipsometer (J.A. Woollam Co). The high deposition temperature poses some fabrication and integration restrictions, similar to LP-CVD Si_3N_4. The materials beneath the TiN layer must withstand the TiN-deposition and etch conditions without degradation. Since the properties of the TCO degrade at high temperatures, the TCO layer must be deposited only after the deposition and patterning of the TiN layer.

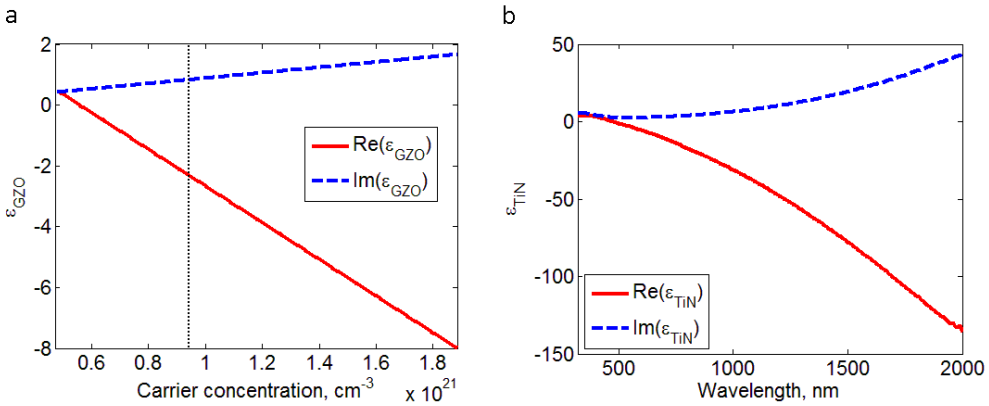

Fig. 3. (a) GZO permittivity versus its carrier concentration, $\lambda = 1.55$ μm. The permittivity of the GZO layer was taken from [52] and a carrier concentration in the GZO was determined using a Drude-Lorentz model fitting: $N_0 = 9.426 \times 10^{20}$ cm^{-3} (black dotted line). (b) TiN permittivity extracted from spectroscopic ellipsometry measurements.

In all cases, we consider the one-dimensional structure as an approximation to the two-dimensional stripe waveguide. This assumption does not substantially affect the theoretical performance of the devices [5, 58]. The thickness of the internal GZO, TiN, SiN, Si_3N_4 layers is 10 nm. The top and bottom cladding layers are assumed to be infinitely thick.

5. Defining the figure of merit

Before defining the FoM used in our analysis, a few fundamental parameters should be discussed. First of these is the mode size. Due to the complex field profiles of the multilayer structures, we define the mode size such that 86% of electrical energy is localized within the region as shown in Fig. 4. This is similar to the case of a single interface where the 1/e point of the electric field corresponds to an 86% localization of electrical energy.

The second parameter is the attenuation of the signal in decibels, which is calculated from the absorption coefficient as $\alpha = 8.68\,\mathrm{Im}(\beta_{\mathrm{eff}})$ [17], where β_{eff} is the complex propagation constant of plasmonic wave in the multilayer structures. Therefore, the extinction ratio (ER) of the modulator is defined as

$$ER = \alpha_{\max} - \alpha_{\min}, \tag{1}$$

#194460 - $15.00 USD Received 26 Jul 2013; revised 17 Oct 2013; accepted 18 Oct 2013; published 4 Nov 2013

where α_{min} is propagation loss in the off-state and α_{max} is the maximum of the propagation loss in the on-state. Here, we define the on-state as the carrier concentration which results in the maximum absorption in each modulator design.

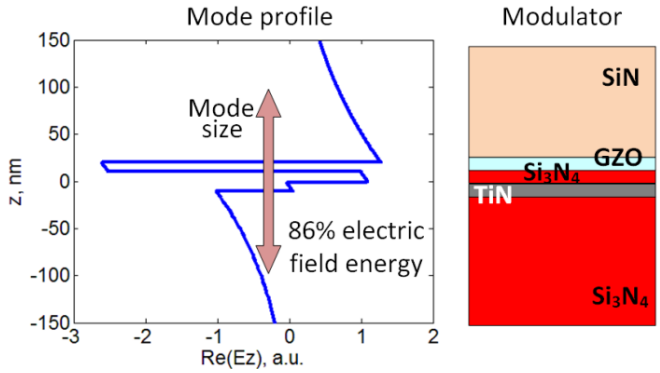

Fig. 4. Depiction of the mode profile illustrating the definition of the mode size. Due to the complexity of the structure and high concentration of electrical energy in the GZO layer, the traditional definition of the mode size cannot be utilized. Here we define the mode size as the distance/range, which encompasses 86% of the electric field energy, a condition similar to that of the 1/e definition for a single interface waveguide.

We define the off-state as the minimum in the absorption. However, two solutions are possible. For this discussion, we consult Fig. 5 which illustrates the absorption coefficient and mode size as a function of carrier concentration for each of the six structures. Note that the final structure, Fig. 2(f) supports both a symmetric and asymmetric mode. As shown in Figs. 5(a) and 5(c), a reduction in the absorption can be achieved either by increasing or decreasing the carrier concentration from the on-state (α_{max}). However, as shown in Figs. 5(b) and 5(d), for $N < N(\alpha_{max})$, the plasmonic mode becomes delocalized from the waveguide, resulting in a drastic increase in the mode size. This scenario is highly undesirable because 1) the delocalized light can result in significant cross-talk between devices, and 2) the light may recouple to the plasmonic waveguide resulting in reduced modulation capability. Thus, we refer to the off-state as $N_{off} = 2N_0 = 1.88 \times 10^{21}$ cm^{-3}.This definition is valid for all the proposed structures apart from Si_3N_4/GZO/SiN/ZnO in Fig. 2(a) due to its small range containing a bound mode (see Fig. 5(b)). Thus, for this layout, $\alpha_{min} = \alpha$ ($N = 8 \times 10^{20}$ cm^{-3}) is defined.

Finally, we define a FoM for such multilayer modulator structures as

$$\mathrm{FoM} = \frac{ER}{\alpha_{min}} \frac{\lambda_{eff,off}}{w_{off}} \tag{2}$$

where ER is the extinction ratio, α_{min} is the off-state absorption coefficient, $\lambda_{eff,off} = 2\pi / \mathrm{Re}(\beta_{eff})$ is the effective wavelength in the modulator in the off-state, and w_{off} is the off-state mode size. This FoM reflects the trade-off between the modulation depth and the loss of the signal in the off-state (α_{min}), while giving additional weight to devices which can fulfill the promise of plasmonics, compactness.

6. Modulator performance

A summary of the performance parameters for the investigated structures are shown in Table 1. The highest FoM is obtained by the high-index "thin TiN" structure in Fig. 2(f). This modulator can outperform previously proposed designs whose performance is shown in Table 2. The increase in the FoM for our devices largely stems from the increase in the ER. Of the top three performing devices discussed here (all high-index cladded structures), the ERs are

#194460 - $15.00 USD Received 26 Jul 2013; revised 17 Oct 2013; accepted 18 Oct 2013; published 4 Nov 2013

up to twice the highest ER obtained in previous works. This is largely due to the fully plasmonic nature of the devices. In this case, the dynamic layer is able to be placed very near the field maximum, or may in fact support the SPP. This greatly increases the effect of the permittivity modulation on the SPP wave. However, because these devices are able to detune from the plasmonic resonance, the absorption coefficient in the off-state can be relatively low while maintaining a mode size on the order of λ_{eff}.

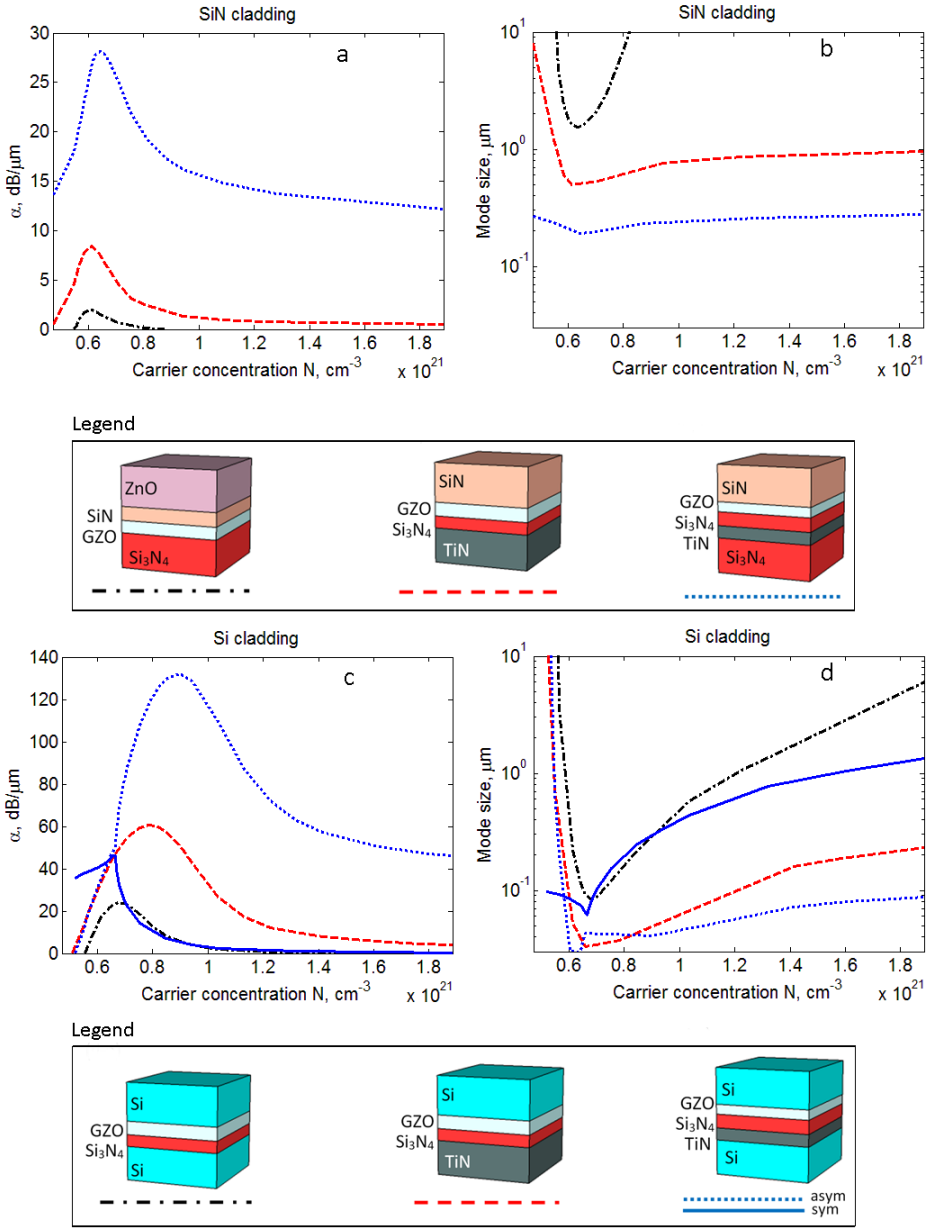

Fig. 5. Multilayer structures along with graphs of the absorption coefficient (a, c) and mode size (b, d) versus GZO carrier concentration. Structures with high-index cladding (lower) show much higher absorption than structures with a low-index cladding (upper). The absorption maximum is accompanied by the highest mode localization, which occurs at the plasmon resonance for the structure. At lower carrier concentrations in the GZO, modes are increased due to smaller magnitude of its real permittivity.

#194460 - $15.00 USD Received 26 Jul 2013; revised 17 Oct 2013; accepted 18 Oct 2013; published 4 Nov 2013

The high-index structure shown in Fig. 2(f), achieves off-state losses of 0.29 dB/μm while maintaining a large *ER* of 46 dB/μm. This structure obtained the largest FoM = 51, approximately twice the FoM of all other structures shown here. This large *ER* requires only a 65 nm of modulator length to achieve a 3 dB signal modulation. This is the only structure considered in the subsequent integration analysis.

Table 1. Performance comparison for planar modulator designs. In the following table all of the fundamental parameters for the device characterization are listed. Among them we have N_{on} which is the on-state carrier concentration, α_{max} which is the maximum absorption in the on-state, α_{min} which is the minimum absorption in the off-state, *ER* is the extinction ratio as defined in Eq. (1), w_{off} is the off-state mode size, n_{eff} is the effective index of the mode, and FoM is the figure of merit as defined in Eq. (2).

Structure (layers bottom to top)	N_{on}, 10^{20} cm^{-3}	α_{max}, dB/μm	α_{min}, dB/μm	*ER*, dB/μm	w_{off}, μm	n_{eff}	FoM
Si_3N_4/GZO/SiN/ZnO Fig. 2(a)	6.1	1.95	0.11	1.8	10	1.96	1
TiN/Si_3N_4/GZO/SiN Fig. 2(b)	6.1	8.4	0.50	8	1.0	1.83	13
Si_3N_4/TiN/Si_3N_4/GZO/SiN Fig. 2(c)	6.4	28	12.2	16	0.3	2.7	3
Si/Si_3N_4/GZO/Si Fig. 2(d)	6.8	24	0.06	24	6	3.5	30
TiN/Si_3N_4/GZO/Si Fig. 2(e)	7.8	60	4.2	56	0.2	3.7	24
Si/TiN/Si_3N_4/GZO/Si Fig. 2(f), asym	9.0	132	46	86	0.09	6.8	5
Si/TiN/Si_3N_4/GZO/Si Fig. 2(f), sym	**6.6**	**46**	**0.29**	**46**	**1.3**	**3.6**	**51**

Table 2. Summary of the performance of previous works in TCO based modulator structures. This is for means of comparison with the structures presented in this paper.

Device	*ER*, dB/μm	α_{min}, dB/μm	λ, nm	w_{off}, μm	n_{eff}	FoM
Lu-Shi [36]	18	1.0	1310	0.3	2.0	39
Sorger-Zhang [19]	1	0.04	1310	0.35	3.0	32
Huang-Sorger [20]	6	0.7	1310	0.2	3.0	19

7. Waveguide-modulator integration and losses

To achieve the highest performance of the integrated structure, the ability to efficiently couple into the device is critical. Ease of integration and coupling losses were considered from the beginning of the design, evident by our use of the low-loss stripe waveguide geometry as a template. Because of this, very efficient coupling can be achieved both into and out of the modulator. A schematic of the high-index "thin TiN" modulator structure integrated with high-index cladded TiN stripe interconnects is shown in Fig. 6. To achieve a similar mode size between the high-index modulator and interconnects, silicon was also used as the cladding for the waveguides. However, to prevent electrical shorting of the modulator structure, p-n junctions must be formed through doping of the silicon [59]. Despite this doping, losses in the silicon are still several orders of magnitude below plasmonic losses, and are neglected in this analysis.

#194460 - $15.00 USD Received 26 Jul 2013; revised 17 Oct 2013; accepted 18 Oct 2013; published 4 Nov 2013

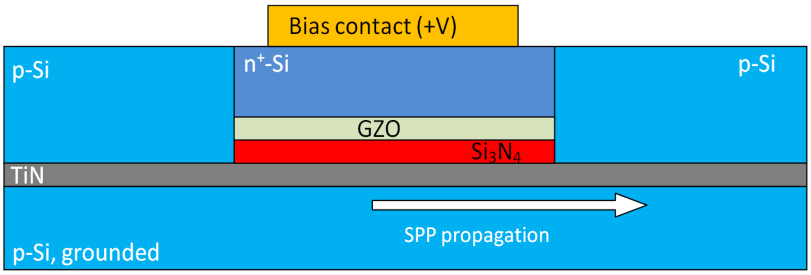

Fig. 6. Schematic of plasmonic modulators integrated with TiN stripe waveguides providing long range SPP propagation to and from the modulator (side view). To create the electrical isolation and prevent shorting of the modulator structure, the silicon layers are doped as shown. However, even with large doping required in the n + region, the losses associated with silicon are several orders of magnitude below the plasmonic losses and are neglected in this analysis.

Similar to the previous sections, we perform calculations for one-dimensional structures as their properties are close to those of finite-width. The coupling loss γ for a single interface was calculated by following equation

$$\gamma = \frac{4\beta_1\beta_2}{(\beta_1+\beta_2)^2}\frac{\left|\int_\infty E_{1z}E_{2z}^*dz\right|^2}{\int_\infty E_{1z}E_{1z}^*dz\cdot\int_\infty E_{2z}E_{2z}^*dz}, \quad (3)$$

where β_1 (E_1) and β_2 (E_2) are the mode indices (electric field) in the waveguide and modulator, respectively. Equation (3) takes into account both the mode overlap integral and the Fresnel coefficients at the boundary region.

We calculated the coupling losses for the design shown in Fig. 6, and the results are shown on Fig. 7. For the off-state (N = 1.88 × 10^{21} cm^{-3}) coupling losses are shown to be approximately 0.7 dB for each interface. This, along with the low propagation loss in the modulator structure ensures high signal throughput in the off-state. As the carrier concentration is reduced, the coupling loss monotonically increases towards the maximum in the modulator absorption. The increase in coupling loss is a result of the highly localized field at the plasmon resonance (maximum absorption). In this situation, the field is almost entirely located within the GZO layer leading to a small mode overlap integral and high coupling losses (Fig. 8). This effect can be beneficial for modulator performance in specific applications as it provides additional losses in the on-state and fewer losses in the off-state.

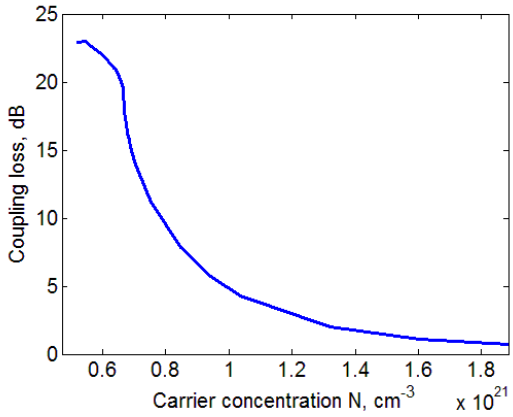

Fig. 7. Single interface coupling loss between the high-index waveguide and high-index "thin TiN" modulator sections versus carrier concentration in the GZO layer.

#194460 - $15.00 USD Received 26 Jul 2013; revised 17 Oct 2013; accepted 18 Oct 2013; published 4 Nov 2013

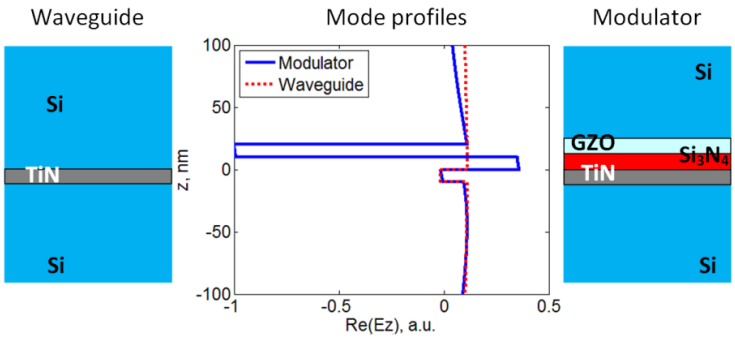

Fig. 8. Example mode profiles in the integrated modulator geometry high-index "thin TiN". Note that the field decay outside the stripe waveguide is slow and therefore appears constant in this graph. The carrier concentration in the GZO layer used for the calculations corresponds to the maximum absorption in the modulator, i.e. plasmonic resonance condition $N = N_{on}$. Under these conditions the majority of the field is localized within the GZO layer.

8. Conclusion

In this paper, we have analyzed several multilayer structures with alternative plasmonic materials to be utilized in ultra-compact, CMOS-compatible plasmonic modulators. Various materials were studied as constituent building blocks of the investigated geometries including different dielectrics (silicon nitride, silicon, zinc oxide) and plasmonic materials such as transparent conducting oxides and titanium nitride. Applying an electric field across the TCO layer allows for the permittivity to be tuned, resulting in a change of the absorption coefficient of the waveguide. Therefore, active modulation is achieved. Numerous modulator layouts are investigated and the typical trade-off between compactness and propagation loss is analyzed. Amongst all the reported structures, one stands out with a remarkable FoM (even in comparison with the best state-of-the-art devices). This FoM takes into account the modulation depth (ER = 46 dB/μm), propagation losses in the off-state (α = 0.29 dB/μm), and off-state mode size (w_{off} = 1.3 μm). The corresponding geometry may allow for ultra-compact modulation with effective length much less than 1 μm. The proposed approach based on the cost-effective planar fabrication processes and the ability to easily integrate with existing semiconductor systems could enable new devices for applications in on-chip optics, sensing, optoelectronics, data storage, and information processing.

Acknowledgments

We thank Jieran Fang, Jongbum Kim, and Naresh K. Emani for helpful discussions. V.E.B. acknowledges financial support from 2012 SPIE Optics and Photonics Education Scholarship, Otto Mønsteds and Thomas B. Thriges foundations. M.F. wishes to acknowledge the Marie Curie Outgoing International Fellowship (contract no. 329346). A.V.L. acknowledges partial financial support from the Danish Research Council for Technology and Production Sciences via the THz COW project. We acknowledge support from the following grants: ARO grant 57981-PH (W911NF-11-1-0359), NSF MRSEC grant DMR-1120923 and NSF PREM DRM-0611430.